On The Generation Mechanism of The X Phase

by Wataru MORII

Abstract

From the May 23, 1989 Macquarie Ridge earthquake, repetitions of the X phase were clearly recorded by the long period seismic wave observation system in operation at the Osakayama Crustal Deformation Observatory. The wide dynamic range and the special triggering algorithm of the system allowed recording repetitions from the first order to 6th order. Though the X phase is treated as a packet of spheroidal overtones a priori and utilized to estimate geophysical parameters, however, its generation mechanism has not been investigated in detail. In this paper, it was attempted to clarify the generation mechanism of the X phase. The records obtained were corrected with deconvolution filters in the time domain in order to minimize the influence of instrumental response characteristics. Spectra, particle motion, travel times and apparent velocities were examined. It was concluded that X_1 and X_2 are composed of successive arrivals of converted body waves, and X_4 may be a packet of spheroidal overtones.

1. Introduction

From the 1989 Macquarie Ridge earthquake, the X phases were clearly recorded at Osakayama Crustal Deformation Observatory (situated in the central part of the Kinki district, hereinafter being abbreviated "OSK"). The record was obtained by a long period seismic wave observation system which was developed to record higher order repetitions. The wide dynamic range and the special triggering algorithm of the system allowed recording the repetitions of the X phase from the first order to 6th order successively.

X phases were first recognized by Jobert et al (1977)[1] and some features of the phase were pointed out as follows. The oscillation of the X phase polarizes in the direction parallel to the great circle path and the amplitude of the vertical component is very small compared with the amplitude of the longitudinal one. The group velocity changes from 7.5km/sec to 5.5km/sec. The predominant period changes from 40 sec to 200 sec. They explained the original nature of the X phase as follows. Seen as normal modes, they correspond to the superposition of spheroidal overtones in the period range of group velocity extrema. Seen as body waves, they correspond to interfering arrivals of $_mP_nS$ waves under specific conditions. However, they have not come to a definite conclusion.

Later Jobert (1978)[2] attempted to synthesize X phases as a sum of mantle overtones principally from the branches $_3R$, $_4R$, $_5R$. She showed that as to X_4 (the order 4 repetition of the X phase), the differences between the synthesized and observed seismograms were very slight however, for X_2 discrepancies clearly existed. Since the synthesized

seismogram fits the observed record of X_4, it is not reasonable to attribute the discrepancies between the synthesized and the observed seismograms of X_2 to an incompleteness of the Earth model. It is possible that X_2 is not a packet of spheroidal overtones. In other studies concerned with the X phase[3),4),5),6)] after Jobert (1978), the X phase is treated as a packet of spheroidal overtones a priori and utilized to estimate geophysical parameters. No attention is given to the generation mechanism of the X phase. However, utilizing X phases as data to estimate geophysical parameters without making the mechanism of generation clear may lead to incorrect results. In this study we attempted to clarify the generation mechanism of the X phase, by analyzing the repetitions of the X phase recorded from the Macquarie Ridge earthquake.

2. The long period seismic wave observation system

For the X phase, repetitions such as X_1, X_2, $X_3 \cdots$ are observed. In order to clarify the generation mechanism of the X phase, it is essential to record X phases from the first arrival to higher order repetitions successively. Therefore, for this study, a special observation system is required. The observation system must have a wide dynamic range and an operating system with a special triggering algorithm. In general, as the order of repetitions increases, the amplitude of X_n decreases in geometric ratio. Therefore, in order to obtain high resolution records of repetition from the first order to higher orders, the observation system must have a wide dynamic range. For example, in the record from the Macquarie Ridge earthquake, the amplitude ratio of X_1 to X_6 is more than 50 decibels because X1 contains short period components of large amplitude. Therefore, the observation system must have a dynamic range of more than 90 decibel, so that the resolution of the record is high enough to examine both X_1 and X_6 in detail. In general, on the early part of a long period seismogram, body waves and surface waves propagated along a minor arc, such as G_1 and R_1, are observed successively. On the other hand, on the later part, repetitions appear separately at a long interval of time. For example, repetitions of the X phase from the Macquarie Ridge earthquake were observed on the seismogram at intervals of about 50 minutes. On several occasions, the signal level of the section between one repetition and another is as low as the back ground noise level. Therefore, in order to record higher order repetitions successively, a special triggering algorithm is required. The long period seismic wave observation system which is operating at OSK eliminates these problems using the following techniques.

Figure 1 shows the block diagram of the long period seismic wave observation system operating at OSK. The system consists of a set of seismometers, a signal conditioner, an A/D converter unit, a clock, a visual recorder, a hard disk unit and a computer. The computer controls the entire system for data acquisition, using a triggering algorithm. The seismometer consists of a vertical component and orthogonal two horizontal components. **Figure 2-a** shows the frequency response characteristic of the seismometer. As shown in **Fig. 1**, the signal conditioner consists of differential amplifiers (first stage), low-pass filters and amplifiers (final stage). In the first stage, out-
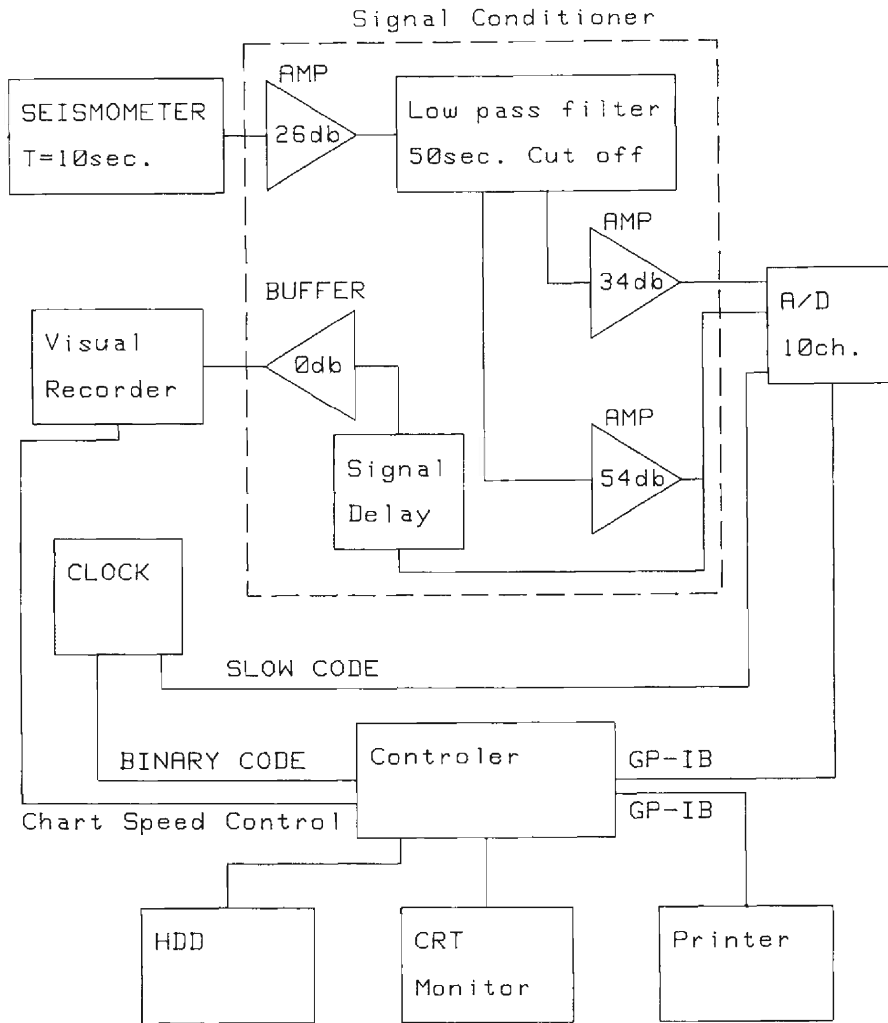
Signal Conditioner

Fig. 1. A block diagram of the long period seismic wave observation system in operation at OSK.

put signals from the seismometer are amplified by 26 decibel. The amplified signals are low-pass filtered at 50 second by the active filter of second order Bessel type, in order to produce an enhancement of long period components. In the final stage, the filtered signal is amplified by 34 decibels and 54 decibels, respectively, so that two-way signals are produced. The frequency response characteristics of the signal conditioner and of the total system are shown in **Figs. 2-b** and -c, respectively.

The computer controls the A/D converter, the visual recorder and the hard disk unit. A flow chart of a control program is shown in **Fig. 3**. Two-way output signals from the signal conditioner are converted to digital data with a 10Hz sampling rate and a quantization of 14 bits. Thus, this system has a dynamic range of 104 decibels in prac-
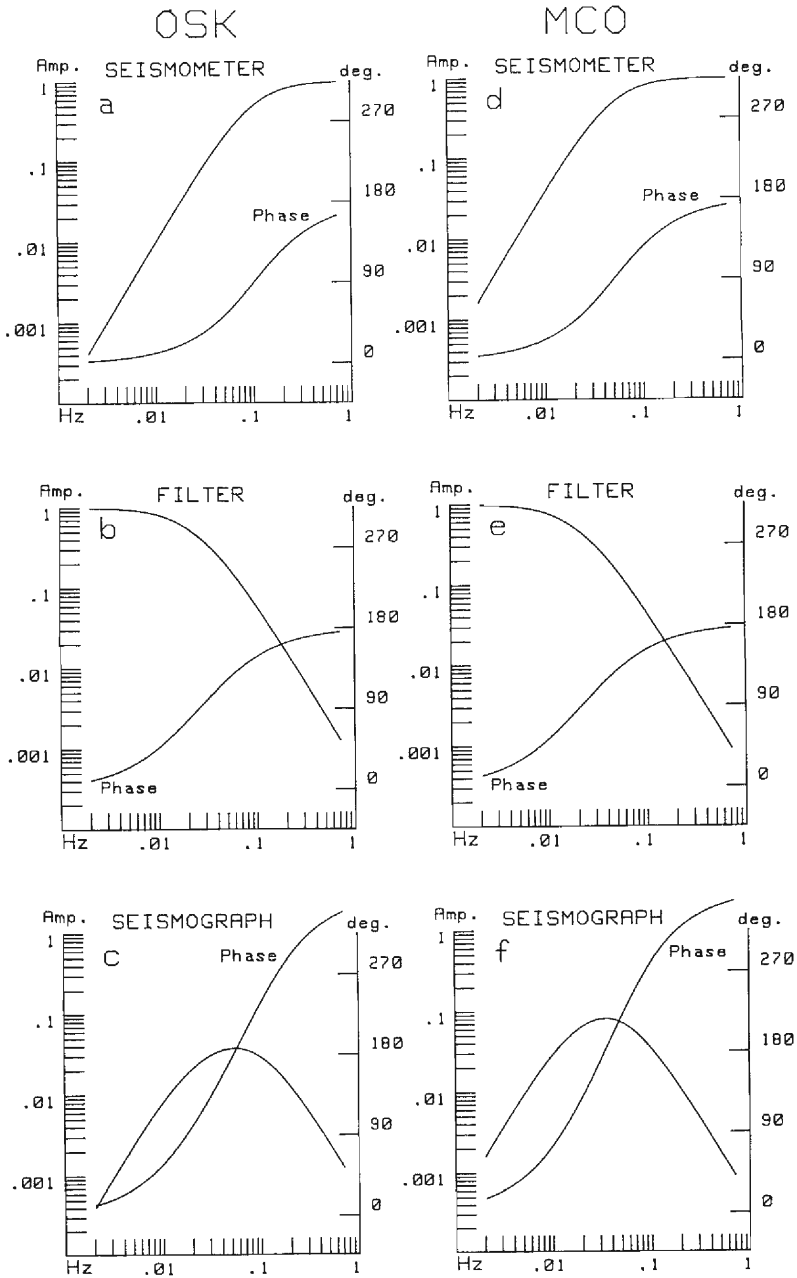
Fig. 2. Frequency response characteristics of the seismographs in operation at OSK and at MCO.

tical use. A/D converted data are transferred to the main memory of the computer via GP-IB interface. Transferred data are stored temporarily in the main memory and usually purged after 60 minutes. However, when the triggering algorithm judges that
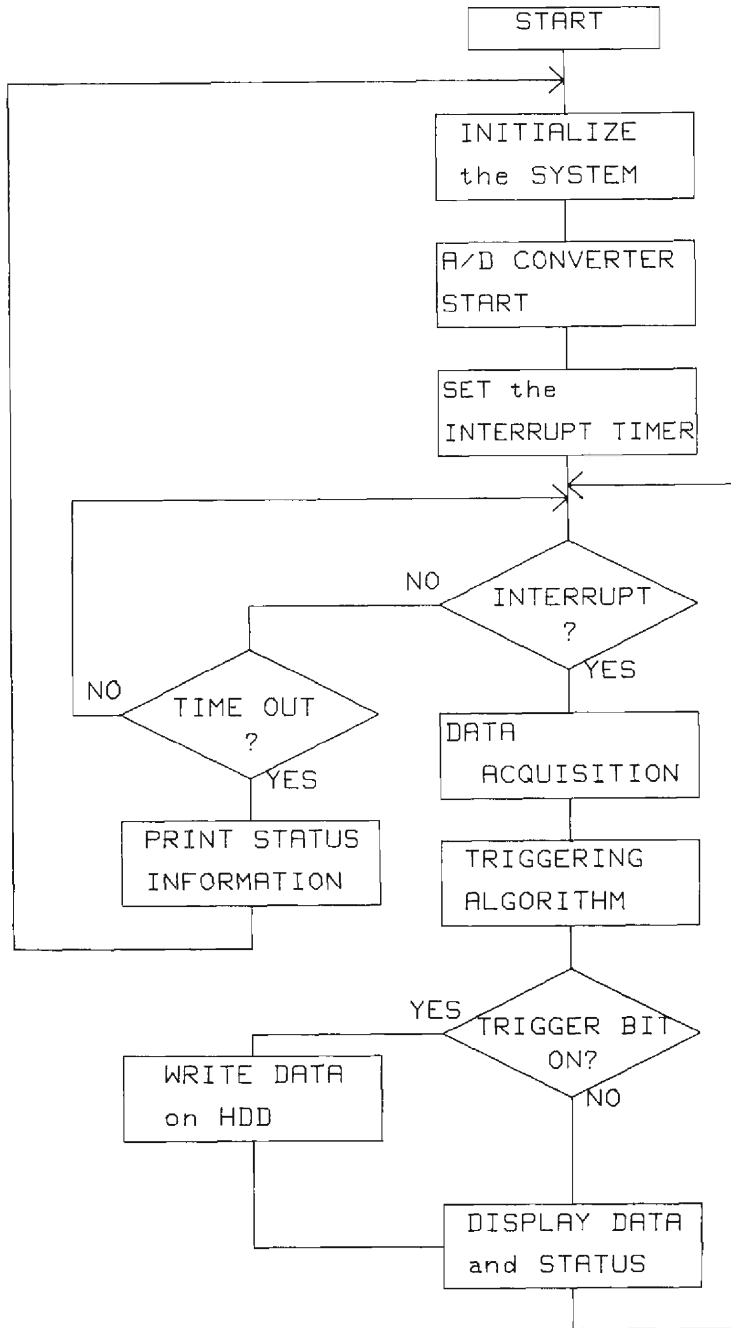
Fig. 3. The flow chart of the control program for data acquisition.

seismic waves are arriving, all the data then stored in the main memory are migrated to a file on the hard disk as delayed data of seismic waves. On the following them, newly sampled data are written in the file continuously until a triggering algorithm judges that no prominent phases will arrive.

The procedure of the triggering algorithm is as follows.

1) In order to eliminate any D. C. offset caused by the signal conditioner, A/D converted data are high-pass filtered at 1000 sec.

2) An average of absolute values over the interval of 5 minutes between t_0-60 minutes and t_0-55 minutes, V_{ref}, is obtained, where t_0 is the latest time of data sampling. The average of background noise, V_{ref}, is used as a standard to judge whether seismic waves are arriving or not.

3) The average of absolute values over the interval of 1 minute between t_0-1 minute and t_0, V, is obtained. When a ratio of V to V_{ref} rises over a fixed rate and the signal is alternate, the triggering algorithm judges that seismic waves are arriving. At the same time, the standard of judgment, V_{ref}, is fixed and this value, $V_{ref-fix}$, is used as the standard to judge whether the earthquake is coming to an end or not.

4) When the ratio of V to $V_{ref-fix}$ falls below the fixed rate continuously for 3 hours, the triggering algorithm judges that no prominent phases will arrive because the difference of arrival time between a repetition of some order, W_n, and a repetition of the next order, W_{n+1}, is not in excess of 3 hours. These procedures are repeated for each sampling of the data.

Since the average of background noise, V_{ref}, is used as the standard of judgment, the triggering algorithm will not take a background noise of large amplitude such as a microseism for a seismic wave. Combined with the apparatus mentioned above, this procedure allows the recording of good quality data useful to analyze repetitions such as R_n, G_n and X_n. For example, when the 1989 Macquarie Ridge earthquake (M=8.2) occurred, X phases were clearly recorded from the first order up to the 6th order successively.

3.   Instrumental correction

As shown in **Fig. 2**, the seismometer and the low pass filter have frequency response characteristics. Therefore, it is necessary to make corrections for the instrumental response before analyzing the records obtained. Fortunately, since the seismometer of the moving coil type and the low-pass filter of the Bessel type are linear response systems to the incoming signal, it is easy to make corrections for instrumental response. Generally, instrumental corrections are performed with Fourier transform in the frequency domain. However, this method is not applicable to transient signals such as seismic waves. **Figure 4** shows the theoretically estimated relation among the acceleration of ground motion, velocity of ground motion and the response of the seismograph. An ideal correction must produce the signal shown in **Fig. 4-b** from the signal shown in **Fig. 4-c**. **Figure 5-b** shows an observed response of a seismograph to the acceleration
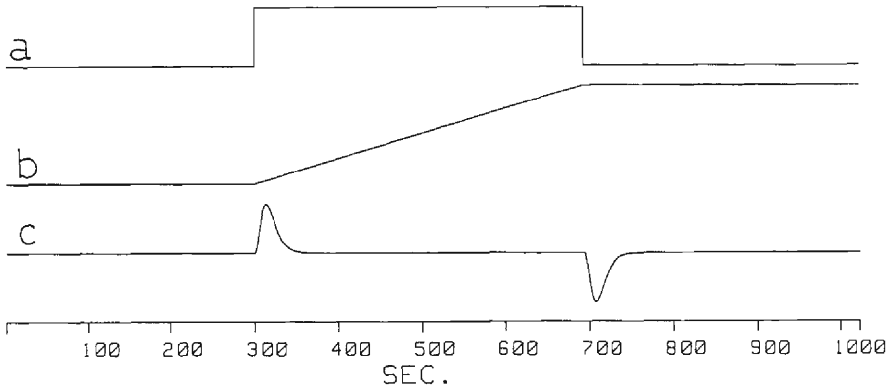
Fig. 4.   Theoretical relation among acceleration of ground motion, velocity of ground motion and response of seismograph.
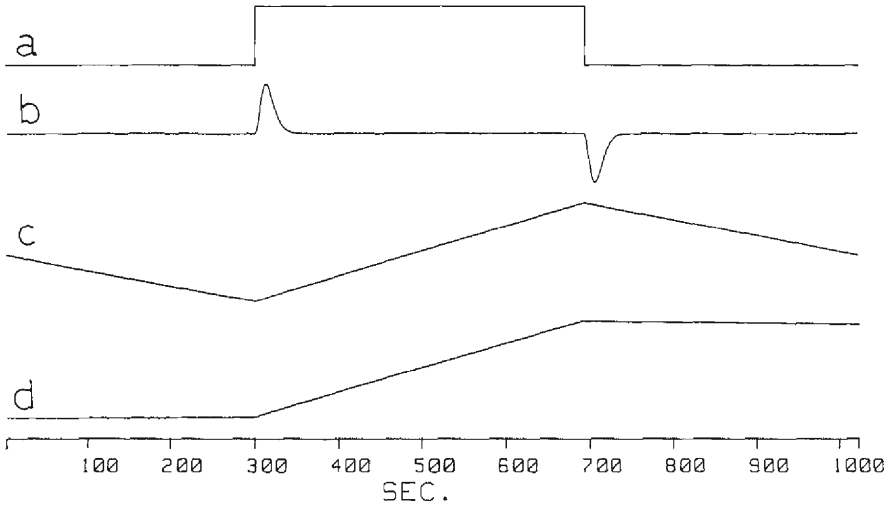

Fig. 5.   Voltage change impressed to a calibration coil (a), response of seismograph (b), and results of instrumental correction with FFT (c) and with deconvolution filter (d).

which is produced by impressing the voltage shown in **Fig. 5-a** to the calibration coil. Utilizing Fourier transform, the signal shown in **Fig. 5-b** was corrected in the frequency domain and the result is shown in **Fig. 5-c**. The signal shown in **Fig. 5-c** is not in agreement with the signal shown in **Fig. 4-b**.

Though defined in the infinite interval, in practical use Fourier transform is applied to a signal of a finite duration. The finite duration of the signal restricts the lowest frequency which can be corrected with Fourier transform to a finite value. As a result, the signal corrected with Fourier transform is just like as a high-pass filtered signal which was ideally corrected. This is a weak point of the operation with Fourier transform.

An instrumental correction performed with the so-called "deconvolution filter" in the time domain is free from this problem.[7] Utilizing a z-transform of the pulse-transfer function, the deconvolution filter is realized as a recursive digital filter.

The impulse response of the seismometer, $h_s(t)$, and that of the low-pass filter, $h_f(t)$, are related to unit impulse function, $\delta(t)$, by the following differential equations, respectively.

$$h_s''(t) + 2\varepsilon h_s'(t) + \varepsilon^2 h_s(t) = \delta(t) \qquad\qquad (1) \; (\textit{for the seismometer})$$
$$A h_f''(t) + B h_f'(t) + h_f(t) = \delta(t) \qquad\qquad (2) \; (\textit{for the low pass filter})$$

where, ε, A and B are parameters that define characteristics of the seismometer and the low-pass filter.

For the low-pass filter, since in the equation (2) $\delta(t)$ is a voltage input and $h_f(t)$ is a voltage output from the low pass filter, desired pulse-transfer function, $F(p)$, is Laplace transform of $h_f(t)$. For the seismometer, in the equation (1), $\delta(t)$ is acceleration of ground motion and $h_s(t)$ is displacement of the pendulum. On the other hand, the output signal from the seismometer is a function of the velocity of a ground motion. The desired pulse-transfer function, $S(p)$, is Laplace transform of $h_s''(t)$. Utilizing Laplace transform, $F(p)$ and $S(p)$ are obtained and the results are as follows.

$$S(p) = p^2/(p+\varepsilon)^2 \qquad\qquad\qquad\qquad\qquad\qquad (3)$$
$$F(p) = 1/(A \cdot p^2 + B \cdot p + 1) \qquad\qquad\qquad\quad (4)$$

Bilinear transforms of $S(p)$ and $F(p)$ are obtained by substituting

$$p = (1 - Z^{-1})/(1 + Z^{-1}) \qquad\qquad\qquad\qquad (5)$$

into equation (3) and (4), respectively.

$$S(Z) = (b_0 + b_1 Z^{-1} + b_2 Z^{-2})/(1 + a_1 Z^{-1} + a_2 Z^{-2}) \qquad (6)$$
$$b_0 = 1/(1+\varepsilon)^2$$
$$b_1 = (-2)/(1+\varepsilon)^2$$
$$b_2 = b_0$$
$$a_1 = (-2)(1-\varepsilon)/(1+\varepsilon)$$
$$a_2 = ((1-\varepsilon)/(1+\varepsilon))^2$$

$$F(Z) = (b_0 + b_1 Z^{-1} + b_2 Z^{-2})/(1 + a_1 Z^{-1} + a_2 Z^{-2}) \qquad (7)$$
$$b_0 = 1/(1+A+B)$$
$$b_1 = 2/(1+A+B)$$
$$b_2 = b_0$$
$$a_1 = 2(1-A)/(1+A+B)$$
$$a_2 = (1+A-B)/(1+A+B)$$

Using the coefficients of equation (6) (or (7)), the n-th sample of input signal, x_n, is related to the n-th sample of output signal from the seismometer (or the low pass filter), y_n, by the following equations.

$$x_1 = y_1/b_0$$

$$x_2 = (y_2 + a_1 y_1 - b_1 x_1)/b_0$$
$$x_n = (y_n + a_1 y_{n-1} + a_2 y_{n-2} - b_1 x_{n-1} - b_2 x_{n-2})/b_0 \quad (n = 3, 4, 5 \cdots\cdots)$$

This is a deconvolution filter.

Figure 5-d shows the signal which is corrected by using the deconvolution filter in the time domain. The signals shown in **Fig. 5-d** and in **Fig. 4-b** agree precisely. This result shows that the deconvolution filter ideally corrects phase-and amplitude-distortions caused by the response characteristics of the seismometer and low-pass filter. These facts demonstrate that the operation with the deconvolution filter provides a better result than the operation with Fourier transform. CPU times needed for operation with the deconvolution filter and for operation with Fourier transform (FFT) are comparable. Hereafter, instrumental collection of records should be performed with the deconvolution filter in the time domain.

4. Data

Records from the May 23, 1989 Macquarie Ridge earthquake were analyzed. They were recorded by the long period seismic wave observation system operating at OSK and by the long period seismograph operating at Miyazaki Crustal Movement Observatory (situated in the southeastern part of Kyushu district, hereinafter being abbreviated "MCO"). The frequency response characteristics of the seismograph at MCO is shown in **Figs. 2-d, -e** and **-f. Figure 6** shows the great circle path corresponding to the Macquarie Ridge earthquake recorded at OSK. The epicentral distance is 9980.2km from OSK and is 9753.3km from MCO. **Figure 7** shows the vertical, longitudinal and transversal components of the seismogram recorded at OSK from the
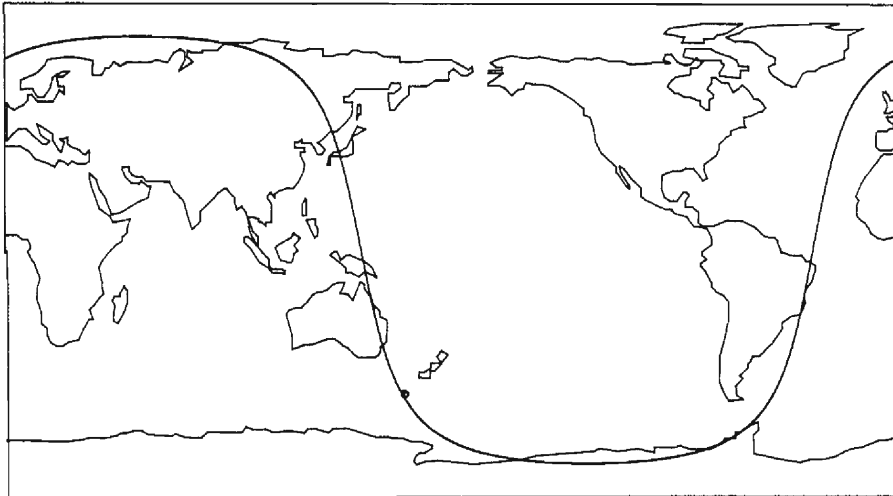

Fig. 6. The great circle path corresponding to the May 23 1989 Macquarie Ridge earthquake recorded at OSK.
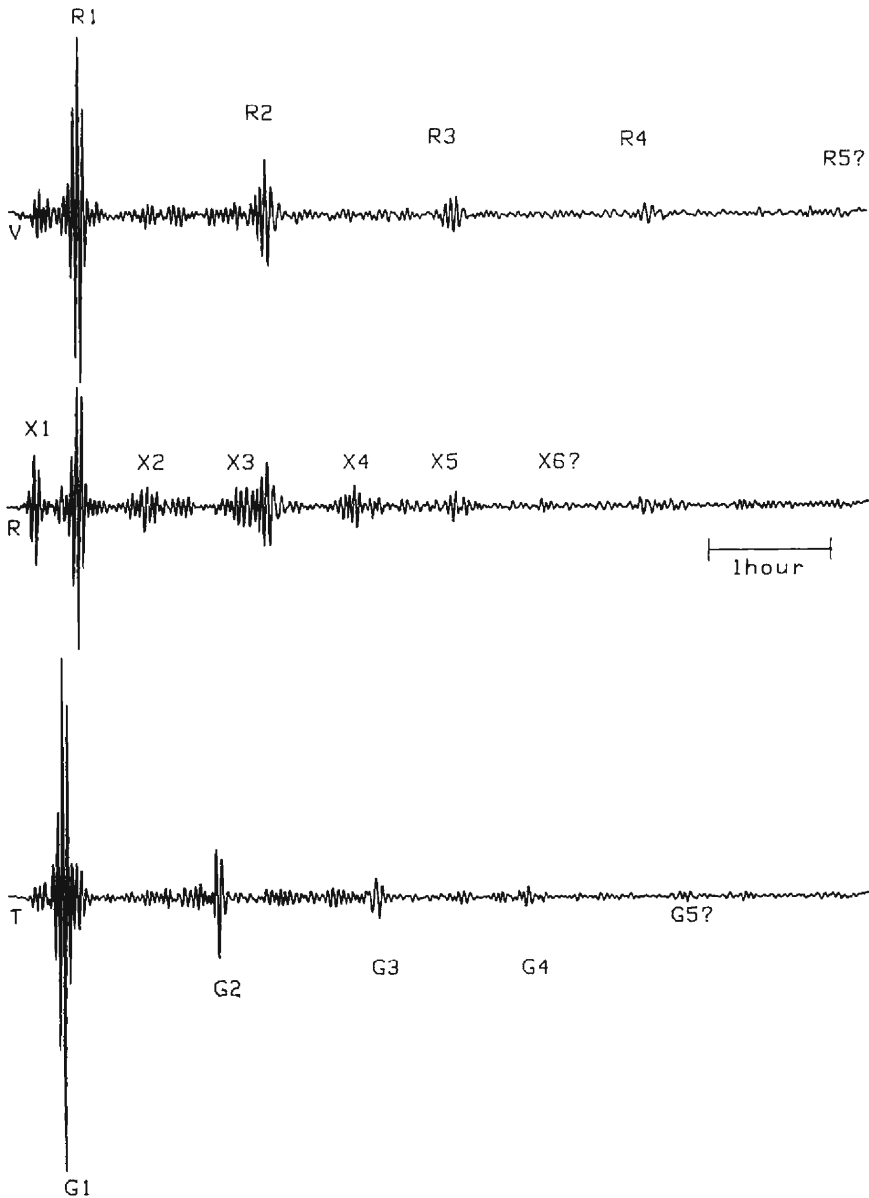
W. MORII

Fig. 7. Vertical, longitudinal and transversal components of the seismogram recorded at OSK from the Macquarie Ridge earthquake. Seismograms are produced by performing a low-pass filtering operation at 100 second and a coordinate transformation.

Macquarie Ridge earthquake. These seismograms were produced by performing a low-pass filtering operation at 100 seconds and a coordinate transformation, so that each repetition is easily identifiable visually. The low-pass filter used is a phase-distortionless

digital filter[8]) with -34 db/octave decay rate. Though the amplitudes of X phases are small in comparison with the amplitudes of R_1 or G_1, the wide dynamic range of the system at OSK allows recording X phases from the first order to the 5th order with enough resolution for the analysis. Moreover, on the original records, X_1 and X_2 phases have larger amplitudes rather than the amplitudes exhibited in **figure 7** because the predominant period of X_1 and X_2 phases are shorter than the cut off period of the filter used. The original records were corrected for the instrumental response characteristics with the deconvolution filters, and are analyzed.

5. Analysis

5.1 Spectra

Figure 8 shows the amplitude spectra of the X phases. Since X_3 and X_5 overlapped with the repetitions of the Rayleigh wave, reliable values of the amplitude spectra of X_3 and X_5 could not be obtained. Though visually discernible on the seismogram, the amplitudes of X_6 phase were not enough to analyze. The curves shown in **Fig. 8** were normalized individually and do not display the amplitude ratio among X_1, X_2 and X_4. As shown in **Fig. 8**, the amplitude spectra of X_1 and X_2 are similar and have a predominant peak in the period ranging from 50 sec to 60 sec. The predominant period of X_4 is very long in comparison with X_1 and X_2.

5.2 Particle motions

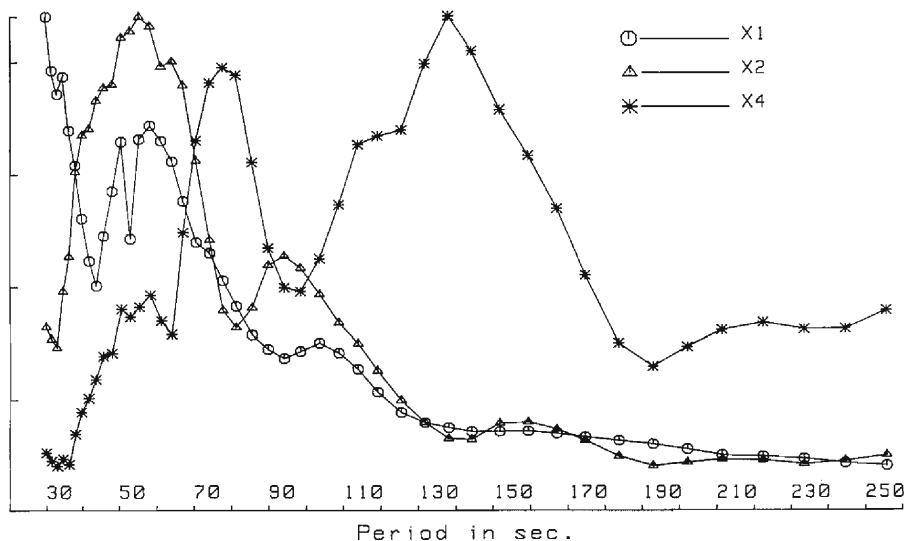For the study of the features of particle motions, vertical and longitudinal com-

Fig. 8. Amplitude spectra of X_1, X_2 and X_4. Curves are normalized individually and do not display the amplitude ratio among X_1, X_2 and X_4.

ponents are band-pass filtered in the period ranging from 38 sec to 220 sec, which produced an enhancement of the X phases. This period range of the band-pass filter includes the periods which were pointed out by Jobert as properties of X phases and correspond to the peaks of amplitude spectra exhibited in **Fig. 8**.

Figure 9 shows the longitudinal component of X_2 recorded at OSK and particle orbits in the vertical plane parallel to the direction of the epicenter. As shown in **Fig. 9**, in the sections denoted by B and D on the seismogram where the amplitude of the longitudinal component is remarkably large, the particle orbits exhibit simple and linear oscillation. In these sections the amplitude and the polarization characteristics of oscillation are explicable as body waves of multiple reflection and conversion, which propagate along the major arc of the great-circle path.
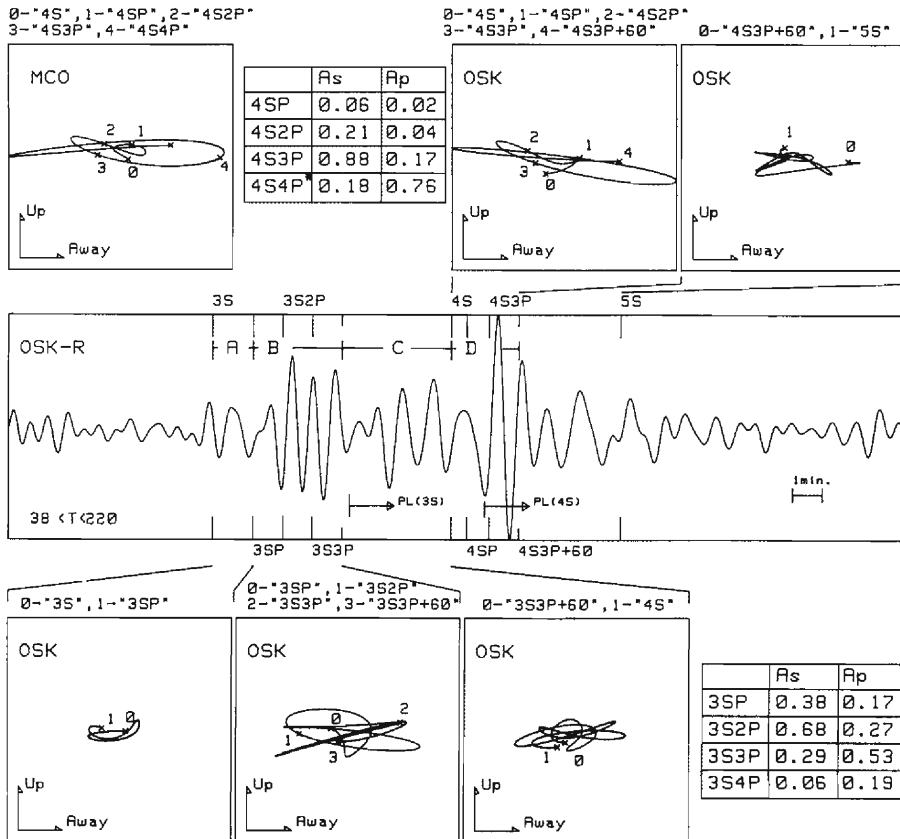
	As	Ap
4SP	0.06	0.02
4S2P	0.21	0.04
4S3P	0.88	0.17
4S4P	0.18	0.76

	As	Ap
3SP	0.38	0.17
3S2P	0.68	0.27
3S3P	0.29	0.53
3S4P	0.06	0.19

Fig. 9. A longitudinal component of X_2 recorded at OSK, particle orbits in the vertical plane parallel to the direction of the epicenter and tables of relative amplitude of $_mS_nP$ estimated theoretically. In the tables, the column denoted by "As" show the amplitude of $_mS_nP$ polarization of which is just like SV wave and the column denoted by "Ap" shows the amplitude of $_mS_nP$ polarization of which is just like P wave. Theoretically estimated arrival times of $_mS_nP$ are exhibited on the seismogram and particle orbits. An particle orbit of a part of X_2 recorded at MCO is also shown to make a comparison.

As generally known, there are converted waves which show different polarization of oscillation from each other but arrive at the same time. For example, SSP and SPS arrive at the same time. The SSP polarizes just like a P wave. On the other hand, the SPS polarizes just like an SV wave. Moreover, the amplitude of SSP is different from that of SPS in relation to coefficients of reflection and conversion. Though the emergent angle of SSP and SPS from the source are the same, reflection coefficients of $S \to S \to P$ conversion is different from those of $S \to P \to S$ conversion. Tables in **Fig. 9** show the relative amplitude of waves of multiple reflection and conversion, $_mS_nP$, where the columns denoted by "As" show the amplitude of waves polarizing as SV waves and the columns denoted by "Ap" show the amplitude of waves polarizing as P waves. These values were estimated theoretically with the PEM-O model[9] and normalized by the amplitude of the S wave radiating from the source. Among $_3S_1P$, $_3S_2P$ and $_3S_3P$, differences of emergent angles from the source were less than 1 degree. Among $_4S_1P$, $_4S_2P$, $_4S_3P$ and $_4S_4P$, differences of emergent angles from the source were less than 2 degrees. It may be not necessary, therefore, to take account of the radiation pattern. According to the theoretical estimation of amplitude, in the early part of the section denoted by B in **Fig. 9**, oscillation polarizing as the SV waves must be predominant and in the later part of the same section, oscillation polarizing as P waves must be predominant. The particle orbits exhibited in **Fig. 9** demonstrate that the theoretical estimations are in agreement with the observed results. Arrival times of each $_mS_nP$ were estimated theoretically with the PEM-O model and marked on the particle orbits. As shown in **Fig. 9**, the time at which changing of the polarization of the observed wave occurred is consistent with the arrival time of each $_mS_nP$ estimated theoretically. In the same manner as section B, the features of particle motions in section D can be explained by successive arrivals of converted body waves, $_mS_nP$. Since, according to theoretical estimation with the PEM-O model, OSK is in the shadow zone as to $_4S_4P$, it follows that in section D, the converted wave polarizing as P waves could not have arrived at OSK. On the other hand, at MCO, which is out of the shadow zone as to $_4S_4P$, the observed waves polarized just as P waves after the theoretically estimated arrival time of $_4S_4P$.

As mentioned above, in the early part and later part of X_2, which are denoted by B and D in **Fig. 9**, the features of particle motion are explained by successive arrivals of converted body waves, $_mS_nP$. However, in section C where amplitude is considerably large, successive arrivals of converted body waves, $_mS_nP$, can not explain the features of oscillation. According to the theoretical estimation, converted waves the arrival time of which match with phases in section C are $_3S_9P$ or so, but large amplitude of the wave train in the section C can not be explained by such phases. Another mechanism of generation must be considered then for the phases which appear in section C.

Figure 10 shows the longitudinal component of X_1 recorded at OSK and the particle orbits in the vertical plane parallel to the direction of the epicenter. As shown in **Fig. 10**, the early part of X_1 is composed of direct S and SP waves, which propagate along the minor arc of the great-circle path. The extremely large amplitude of SP waves is produced by the focusing of seismic rays, in relation to the epicentral distance. **Figure 11** shows seismic rays which were estimated theoretically with the PEM-O model

based on the ray theory. Widely spread S waves focus on the observation point after con-
verting to P waves. The long period pulse with large amplitude in the latest part of X_1
polarized just like SV waves and the arrival time of which coincided with that of SS or
SPS phase. The difference in travel times between the SS and SPS phases is less than 1
second because the SPS wave propagates through almost the entire path (99.8%) in the
form of S waves. According to the theoretical estimation with the PEM-O model, this
phase may be the SPS phase. In this case, the reflection coefficient of S → S conversion
is very small. On the other hand, the reflection coefficients of S → P → S conversions
are large. According to the theoretical estimation with the PEM-O model, S → P → S
conversions conserve about 97% of SV-wave energy radiating from the source. SS-
wave inherits less than 3% of SV-wave energy radiating from the source. Then, SPS-
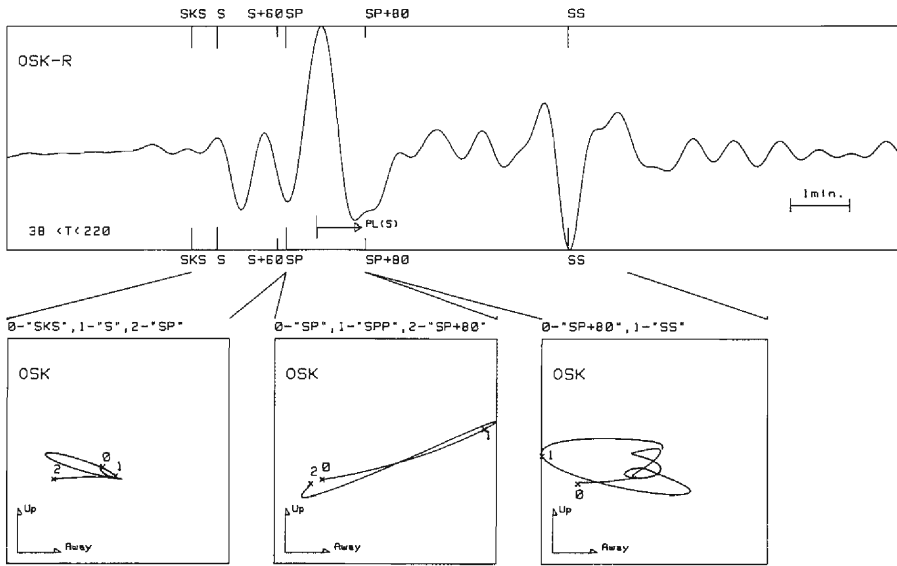wave may be predominant on the seismogram, and SS-wave may be inconspicuous.

Fig. 10.   A longitudinal component of X_1 recorded at OSK, particle orbits in the vertical plane parallel to
the direction of the epicenter. Theoretically estimated arrival times of $_mS_nP$ are exhibited on the
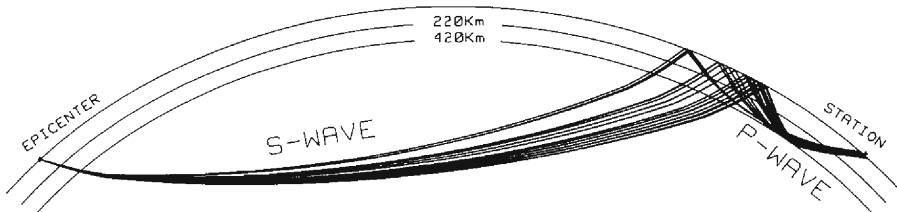seismogram and particle orbits.

Fig. 11.   Seismic rays of SP wave estimated theoretically with PEM-O model based on the ray theory.

As to X_4, features of oscillation could not be explained by the successive arrivals of converted waves. No evident phase of $_mS_nP$ could be identified. It is impossible to treat X_4 by breaking it down into several converted body waves.

5.3 Apparent velocities

The X_2 phases recorded at OSK and at MCO from the Macquarie Ridge earthquake are shown in **Fig. 12**. On the seismograms, corresponding phases at OSK and at MCO are denoted by the same number. Using the time lag between the phases denoted by the same number at OSK and at MCO, apparent velocities were estimated and are shown in **Fig. 12**. The vertical axis indicates the apparent velocity and the horizontal axis indicates the number which is noted on the seismogram to identify the corresponding phase at OSK and at MCO. Apparent velocities of $_mS_nP$ were estimated theoretically with the PEM-O model and are indicated at the right-hand side of the vertical axis. **Figure 12** shows that observed apparent velocities of $_mS_nP$ phases in sections
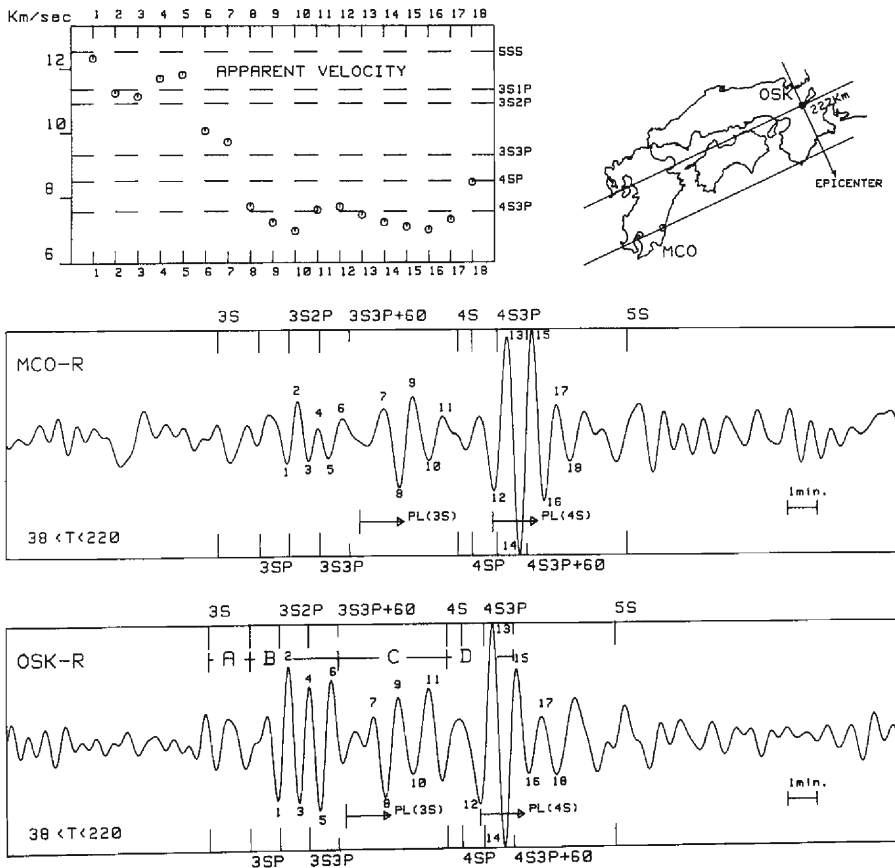

Fig. 12. Longitudinal components of X_2 recorded at OSK and at MCO, and observed apparent velocities of corresponding phases at OSK and at MCO.

B and D are in agreement with the theoretical ones.   Observed apparent velocities of phases in section C, where features of oscillation could not be explained with $_mS_nP$, are similar to those of the phases in section D.

As demonstrated above, the predominant phase in section D is $_4S_3P$.   The seismic ray of $_4S_3P$ was estimated theoretically with PEM-O model and is shown in **Fig. 13**.   As shown in **Fig. 13**, the maximum depth of the rays propagated in the form of P waves are coincident with the 220km discontinuity.   Since observed apparent velocities of waves in section C and in section D are similar, it is supposed that the predominant phase in section C would be a kind of surface wave composed of longitudinal waves trapped in the layer above the 220km discontinuity.   The most likely case is the arrival of PL (SSS).[10],[11]   The arrival time of the wave train in section C is compatible with the well-known property of the shear-coupled PL wave.   The phase velocities of PL wave trapped in the layer above the 220km discontinuity were estimated theoretically with the PEM-O model and are shown in **Fig. 14**.[12]

In order to estimate the phase velocity of dispersive waves with the multiple band-pass filtering method, it is necessary to use a very narrow band-pass filter.[13]   However, immediately before and after section C, waves of large amplitude and similar periods such as $_3S_2P$, $_3S_3P$ and $_4S_3P$ exist.   When the very narrow band-pass filter was used, the influence of these waves could not be suppressed.   Thus, it was impossible to precisely estimate the phase velocity of the waves in section C.   We considered that, as to the wave train in section C, apparent velocities and predominant periods were not much different from the real properties of the phase velocity dispersion.   The theoretical curve indicated 7.7-7.9km/sec in the period ranging between 50 and 55 sec which are the predominant periods of the wave train in section C.   The apparent velocities of the wave
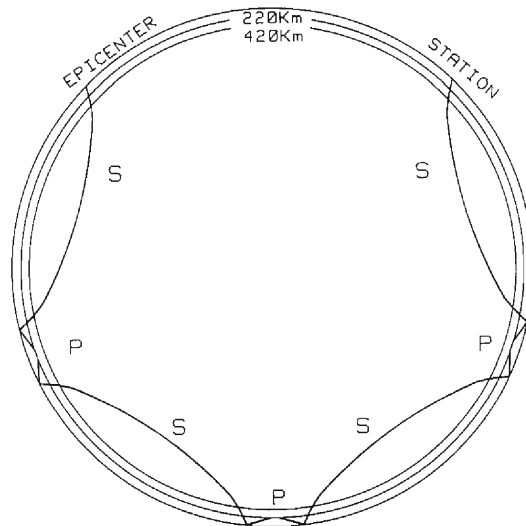

Fig. 13.   A seismic ray of $_4S_3P$ estimated theoretically with PEM-O model based on the ray theory.
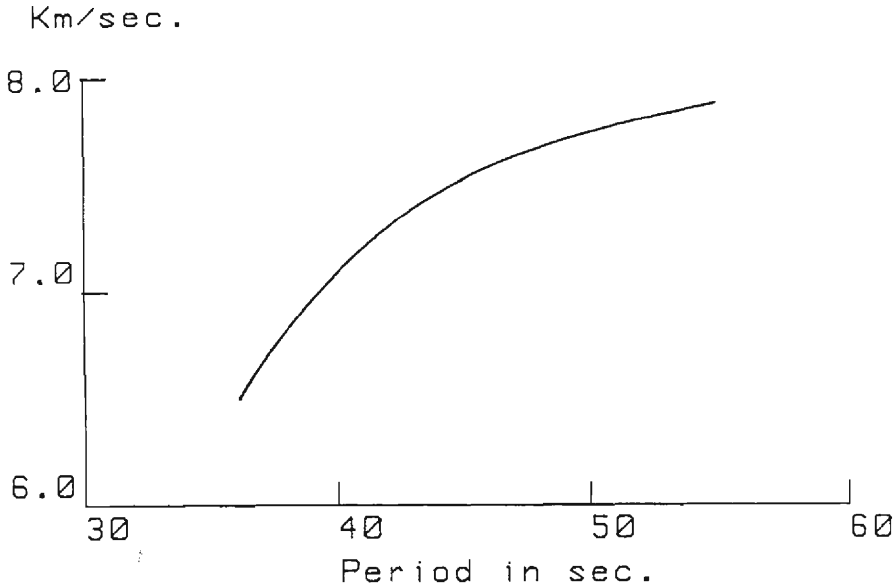
Km/sec.

Fig. 14. A theoretical curve of phase velocities estimated with PEM-O model for PL wave trapped in the layer above 220km discontinuity.

train in section C is 7.0-7.7km/sec. On the theoretical curve, these values corresponded to the phase velocities in the period ranging between 39 and 50 sec. This result shows that properties of the phase velocity dispersion were compatible between the theoretical estimation and the observed one.

6. Discussion

As delineated above, it was demonstrated that the properties of X_1 and X_2 are explained by the successive arrivals of multiple-reflected and -converted body waves. It was also demonstrated that extremely large amplitudes of X_1 are produced by the focusing of SP waves. It was shown that shear coupled PL waves, PL (SSS), form a part of X_2. Comparison of amplitude spectra showed that predominant periods of X_4 differ remarkably from those of X_1 and X_2. No evident phase of converted waves, $_mS_nP$, were identified on the record of X_4. It was impossible to treat X_4 by breaking it down into several converted body waves. Judging from the result shown by Jobert[2], it is adequate to treat X_4 as a packet of spheroidal overtones.

We suppose that X phases display the transient process of differentiation of seismic waves, described as follows. At a discontinuity, a seismic wave radiated from a source separates into different rays because of reflection, refraction and conversion. Further, each of these rays subdivides at another discontinuity. Repeating such subdivision, a seismic wave separates into many different rays, producing a wide variety of phases. The waves which repeatedly underwent only a small number of conversions such as SP,

SPS, etc. are identifiable on a seismogram as body waves and explicable with the ray theory, as shown in the case of X_1 and X_2. On the other hand, after a great number of conversions, such seismic rays are accompanied with small energy and each of them can not be individually identified on a seismogram. It can thus be said that only waves which interfere and intensify each other are recognized on a seismogram as a mode, and are explained with the wave theory in place of the ray theory. X_4 may be generated in such a manner.

Properties of a body wave which repeated only a small number of conversions are mainly affected by the properties of the source process such as a source time function and by the relative position of the source and the receiver. Properties of a mode composed of constructive interferent waves are controlled by the resonant properties of the medium. X_4 may be composed of constructive interferent waves and its properties may be controlled mainly by the resonant properties of the Earth. It may be possible to synthesize X_4 with a simple source time function and several overtone branches, as shown by Jobert.[2] X_1 and X_2 are composed of successive arrivals of converted body waves and they are affected considerably by the properties of the source process and by the relative position of the seismic source and the observation station. It is impossible to synthesize X_1 or X_2 with a simple source time function and only several overtone branches. Good selection of source time functions and making use of a great number of overtone branches may be needed if one attempts to synthesize X_1 or X_2 with modes.

7. Conclusion

The generation mechanism of the X phase was investigated. Spectra, particle motion, travel time and apparent velocities were examined in detail. The results are as follows:

(1) X_1 is composed of the successive arrivals of S, SP and SPS waves. The extremely large amplitude of X_1 is caused by the focusing of SP waves.

(2) X_2 is composed of the successive arrivals of multiple-reflected and -converted body waves. Shear coupled PL waves, PL (SSS), form a part of X_2.

(3) It is impossible to treat X_4 by breaking it down into several converted body waves. It may be adequate to treat X_4 as a packet of spheroidal overtones.

References

1) Jobert, N., R. Gaulon, A. Dieulin and G. Roult: Sur des ondes a tres longue periode, caracteristiques du manteau superieur, C. R. Acad. Sc. Paris, t. 285, ser. B-49, 1977

2) Jobert, N.: Contribution of some particularities in the dispersion curves to numerical seismograms computed by normal modes, J. Comput. Phys., 29, 1978, pp. 404-411.

3) Roult, G. and B. Romanowicz: "Very long-period data from the Geoscope Network" Preliminary results on great circle avarages of fundamental and higher Rayleigh and Love modes, Bull. Seism. Soc. Am., vol. 74, No. 6, 1984, pp. 2221-2243.

4) Emile, A. okal and Bong-Gon Jo: Stacking inversions of the dispersion of higher order mantle Rayleigh waves and normal modes, Phys. Earth Planet. Int., 47, 1987, pp. 188-204.

5) Tanimoto, T.: The three-dimensional shear wave structure in the mantle by overtone waveform inversion-I. Radial seismogram inversion, Geophys. J. R. Astr. Soc., 89, 1987, pp. 713-740.

6) Tanimoto, T.: The 3-D shear wave structure in the mantle by overtone waveform inversion-II. Inversion of X-waves, R-waves and G-waves, Geophys. J., 93, 1988, pp. 321-334.

7) Kulhanek, O.: Introduction to Digital Filtering in Geophysics (Developments in Solid Earth Geophysics 8), Elsevier Scientific Publishing Company 1976

8) Morii, W. and K. Nishimura: Introduction of Library Program (71) — Filtering of Equispace Data —, Bull. Data Processing Center, Kyoto University, 19, pp. 312-318 (in Japanese)

9) Dziewonski, A. M., A. L. Hales and E. R. Lapwood: Parametrically simple earth models consistent with geophysical data, Phys. Earth. Planet. Int., 10, 1975, pp. 12-48.

10) Oliver, J.: On the long period character of shear waves, Bull. Seism. Soc. Am., vol. 51, No. 1, 1961, pp. 1-12.

11) Sergio S. SU and J. Dorman: The use of leaking modes in seismogram interpretation and the PL phase, Bull. Seism. Soc. Am., vol. 55, No. 6, 1965, pp. 989-1021.

12) Oliber, J. and M. Major: Leaking modes and THE PL phase, Bull. Seism. Soc. Am., vol. 58, No. 50, 1960, pp. 165-180.

13) Bloch, S. and A. L. Hales: New techniques for the determination of surface wave phase velocities, Bull. Seism. Soc. Am., vol. 58, No. 3, 1968, pp. 1021-1034.